Journal of Thermal Science Vol.31, No.5 (2022) 1476−1486

https://doi.org/10.1007/s11630-020-1367-2 **Article ID: 1003-2169(2022)05-1476-11**

Experimental Investigation of the Ejector Refrigeration Cycle for Cascade System Application

HAO Xinyue[1,2], GAO Neng[2*], CHEN Guangming[2], VOLOVYK Oleksii[2], WANG Xuehui[3], XUAN Yongmei[2]

1. Institute of Refrigeration and Cryogenics, Zhejiang University, Hangzhou 310027, China
2. Ningbo Institute of Technology, Zhejiang University, Ningbo 315100, China
3. Fluids and Thermal Engineering Research Group, Faculty of Engineering, University of Nottingham, Nottingham NG7 2RD, UK

Abstract: Ejector refrigeration cycle (ERC) with advantages of simple structure and low cost holds great application potential in cascade/hybrid cycles to improve the overall system performance by removing or recovering the heat from the main cycle. In this paper, a theoretical and experimental investigation of the ERC as a part of a cascade system was carried out. The operating parameters were optimized. The experimental ERC test rig was designed, developed and investigated at high evaporating temperatures and wide ranges of operating conditions. The influence of operating conditions on the efficiency of the ejector and ERC was analyzed. Experimental results and analysis in this study can be helpful for the application and operating condition optimization of ERC in cascade/hybrid refrigeration systems.

Keywords: ejector, ejector refrigeration cycle, cascade refrigeration system, experiment, performance

1. Introduction

The mechanical vapor compression refrigeration cycle (VCRC) driven by electrical power is widely used for air-conditioning and refrigeration at the present time. The refrigeration sector consumes about 20% of the overall electricity used worldwide, and a growing amount of the cooling systems and their power consumption will increase [1]. The peaks of the electricity consumption of the cooling systems occur in the summer period when the environment temperature is high and a large amount of cold is needed. Thus, improving the efficiency of the VCRCs with the aim to decrease their power consumption is one of the primary targets.

At the same time, a large amount of waste heat in different forms is discharged to the environment by industry and power generation systems. This waste heat can be utilized to generate the extra cold without additional energy input which surely increases the primary fuel efficiency [2]. Among the various types of thermal refrigeration, the heat-driven ejector refrigeration cycle (ERC) holds great potential in utilizing low-grade thermal energy such as waste or exhaust heat, solar and geothermal energy, etc. [3]. The key component of the ERC is a supersonic ejector which is used as a compression device but has no moving parts. It makes ERC systems simpler in design and operation and more compact than the other types of heat-driven refrigeration systems [4]. However, the ejector compression ratio, as well as its efficiency, is not very high and strongly

Received: Mar 13, 2020 AE: WANG Lin Corresponding author: GAO Neng E-mail: gao@zju.edu.cn

Nomenclature		**Subscript**	
COP	coefficient of performance	C	condenser
ERC	ejector refrigeration cycle	CB	condensation of the bottoming cycle
h	specific enthalpy/kJ·kg^{-1}	CR	compressor
k	coverage factor	D	diffuser
$\dot{m}$	mass flow rate/kg·s^{-1}	E	evaporator of VCRC
P	pressure/MPa	ET	evaporator of ERC
$\dot{Q}$	heat load/kW	FP	feed pump
q	heat load per unit mass/kJ·kg^{-1}	G	generator
T	temperature/°C	M	mixed stream
U_c	expanded uncertainty	MECH	mechanical
u_Y	standard uncertainties	N	nozzle
VCRC	vapor compression refrigeration cycle	P	primary stream
$\dot{W}$	unit power/kW	S	secondary stream
Greek symbol		THERM	thermal
η	efficiency	0	cascade system
μ	entrainment ratio	1,2,3…	state points

depend on the operating conditions. Another reason for the low ejector efficiency is the impact losses. These losses are irreversible and cannot be completely eliminated on the basis of the principle of the ejector operation.

The efficiencies of both the VCRC and ERC depend on the evaporating and condensing temperatures. Decrease of the condensing temperature and increase of the evaporating temperature will improve the COP of the refrigeration systems, but in practice, these temperatures depend on the environment and operating conditions and cannot be easily changed during operation. One of the prospective ways for efficiency improvement is using the electrically-driven VCRC in combination with heat-driven ERC, which can use available waste heat [3]. To improve the COP of the ejector cooling cycle, Sokolov and Hershgal proposed various configurations of a compression-enhanced ejector cooling systems [5]. In the proposed systems, the mechanical compressor is used in different combinations as a buster to increase the ejector suction pressure. From the proposed cycles, the most interesting is cascade cooling cycle which is a combination of the VCRC as a bottoming cycle, and the ERC as a topping cycle, and the two cycles are connected through a common heat exchanger, i.e., the intercooler. Later Sokolov and Hershgal investigated the possibility of using solar energy for the ERC operation, but the overall efficiency for the system was very low due to using the same refrigerant R114 for both cycles [6]. Based on the work of Sokolov and Hershgal, Arbel and Sokolov investigated the cascade cooling system, but only one change was made compared to previous work: the refrigerant was changed from R114 to R142b. The results of investigation indicated that the overall efficiency of the cascade cooling system was increased by 15% to 45% compared with results obtained for the refrigerant R114 [7].

Sun made a detailed analysis of a similar system in air-conditioning mode of operation which used refrigerant R134a for the bottoming VCRC and water for the topping ERC [8]. In the proposed system, the water was directly boiled in the solar collector. The results showed that COP of the cascade cooling system increased by about 50% than that of VCRC. Mansour et al. analyzed several ejector and compressor cycle combinations with refrigerant R134a. Regarding the obtained results, the cascade cooling system can improve the COP of conventional mechanical compression cycle by 40% [9].

With the aim to realize a sub-critical CO_2 cooling cycle, Petrenko et al. proposed an advanced solar-assisted cascade ejector cooling/CO_2 sub-critical mechanical compression refrigeration system [10]. In this system, the topping ERC operating with neopentane as refrigerant was used to condense the CO_2 vapor of the bottoming cycle in the cascade condenser. Based on the obtained results, a pilot small-scale cascade CO_2 sub-critical mechanical compression/ejector refrigerating unit was developed with a cooling capacity of 5 kW. Later, Nesreddine et al. investigated experimentally the similar cascade cooling system which used refrigerant R245fa for the ejector topping cycle in a wide range of operating conditions. The experimental results showed that the efficiency improvement of the single-stage CO_2 systems operating in sub-critical modes can reach up to approximately 45% by using the cascade concept [11].

Sanaye et al. proposed a novel two-step method for

modeling and optimum design of the cascade mechanical compression/ejector cooling cycle which covered both economy and thermodynamic aspects of the system. The results of the cascade cycle optimization showed that the thermal COP and mechanical COP increased up to 41% and 67.5%, respectively [12]. In final, the cost of electrical power consumption for generating one ton of cooling capacity for the cascade system was lower than that of convenient VCRC by 33%. Chen et al. investigated an improved cascade mechanical compression-ejector cooling cycle [13]. In the proposed system with the aim of improving the whole system's efficiency, the superheated CO_2 vapor was used to preheat the working fluid supplied to the vapor generator of the topping ERC. The results showed a small growth (about 1.6%) in the overall mechanical COP due to a very slight decrease in the feed pump power consumption and invariable of compressor power consumption. But at the same time, the overall thermal COP of the system increased by 30% due to decreasing the heat needed from the external source for the topping ejector cycle operation. Also, the analysis showed that the relative decrease in heat loads for the heat exchangers allows decreasing the weight and dimensions of the ejector cooling sub-cycle and the entire cascade system.

It follows from the above that the cascade cooling cycle based on the VCRC and ERC is very prospective. This combination allows improving the efficiency of both cycles. Also, the intercooler or cascade condenser which connects two cycles is only a heat exchanger, permitting the use of different and most suitable refrigerants for each sub-cycle to get the maximum efficiency of the system. At the same time, to provide continuous operation of the cascade cooling system, the topping ejector refrigerating cycle should use a stable source of heat, like waste or exhaust heat, but not solar heat.

The overall COP of the cascade cooling system depends on the COPs of each sub-cycle. The COP of the ERC is very sensitive to the operating conditions, especially the evaporator temperature in the case of utilizing the ERC as the topping cycle of the cascade system. At the same time, the COP of the VCRC depends on the condenser temperature. Since these two temperatures are connected to each other, the optimization of the cascade cooling cycle with the aim to choose optimal design conditions for both sub-cycles is very important.

This research aims to carry out an experimental investigation on the ejector refrigeration cycle intended for cascade system application. Based on the theoretical analysis of the cascade cooling cycle, the design parameters and refrigerant for the ejector cooling cycle were chosen. The experimental ejector and ejector test rig were designed and constructed. The experiment procedure was developed to investigate the ejector and ejector cooling cycle performance. Ejector and ejector refrigeration cycle parameters in a wide range of operating conditions were obtained experimentally.

2. Analysis of the Cascade Cooling Cycle

2.1 Cycle description

A schematic diagram of the cascade refrigeration system is shown in Fig. 1. The electrically-driven VCRC provides cooling capacity for air-conditioning or cold water supply. The heat-driven ERC serves for cooling the condenser of the VCRC. Two cycles are thermally connected through a common heat exchanger: cascade condenser. In this way, the VCRC acts as the main cycle, and the ERC acts as an auxiliary cycle aimed for improving the efficiency of the main cycle. The thermodynamic cycles in *p-h* diagrams are shown in Fig. 2(a) and 2(b).

The operating principle of the cascade refrigerating cycle is presented as follows. The refrigerant vapor is evacuated from the evaporator by the compressor, then compressed and discharged to the cascade condenser. In cascade condenser, the high-pressure refrigerant vapor is liquefied by rejecting heat to the topping cycle refrigerant. The liquid refrigerant leaves the condenser and expands through the expansion valve 1, and then enters the evaporator where it evaporates at low pressure and produces the cooling effect $\dot{Q}_{\mathrm{E}}$ for refrigeration purposes. This completes the bottoming vapor-compression refrigeration cycle.

The liquid refrigerant of the topping cycle is boiled in the vapor generator as a result of the heat supplied from the external heat source. This primary vapor with a mass flow rate $\dot{m}_{\mathrm{P}}$ obtained in the vapor generator passes through the supersonic nozzle of the ejector, is accelerated through nozzle with pressure reduction, and as a result, creates the low-pressure region in the mixing chamber of the ejector. It ensures the suction of the low-pressure secondary vapor of the refrigerant with a mass flow rate of $\dot{m}_{\mathrm{S}}$ from the cascade condenser. The primary and secondary vapor fluids are mixed in the ejector mixing chamber and passes through the ejector diffuser, where the mixture pressure is increased. The compressed mixture with a mass flow rate of $\dot{m}_{\mathrm{M}} = \dot{m}_{\mathrm{P}} + \dot{m}_{\mathrm{S}}$ enters the condenser and is liquified by the heat rejected to the environment. The liquid leaving the condenser is collected in the receiver and then divided into two fluids. One fluid with a mass flow rate of $\dot{m}_{\mathrm{P}}$ is pumped back to the vapor generator by the feed pump. Another one is expended through the expansion valve 2 and enters the cascade condenser where it

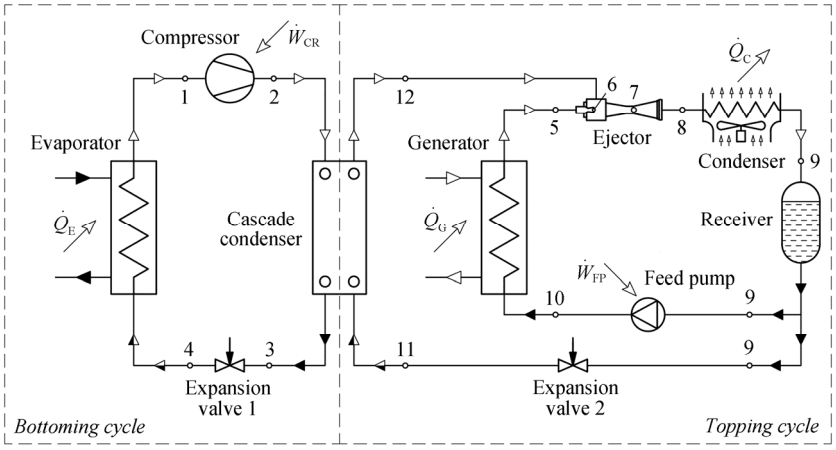

Fig. 1 Schematic diagram of the cascade refrigerating system

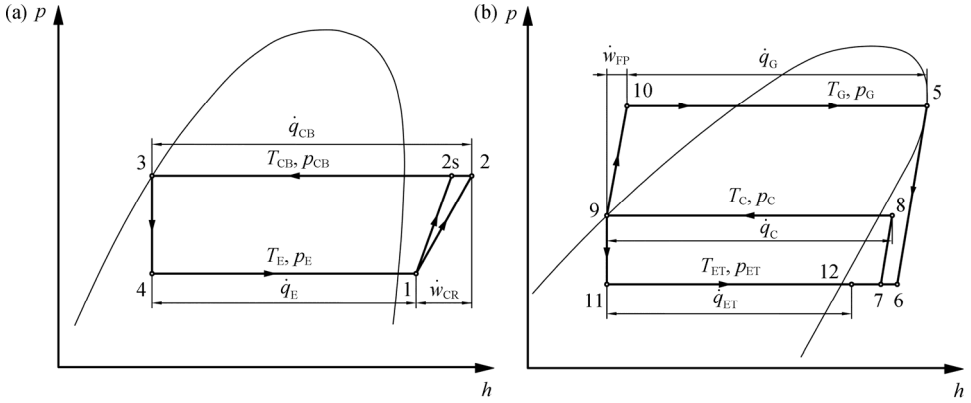

Fig. 2 Vapor compression refrigerating cycle (a) and ejector refrigerating cycle (b) in *p*-*h* diagram

evaporates at low pressure by the heat supplied from the bottoming cycle refrigerant. Finally, the obtained vapor is entrained by the ejector, thus completing the heat-driven ejector cooling cycle.

2.2 Thermodynamic analysis of the cascade cooling cycle

Using the numbering in Fig. 1 and Fig. 2, the analysis of the cascade system is described as follows.

For a given cooling capacity $\dot{Q}_E$, the bottoming refrigerant mass flow rate $\dot{m}_E$ can be defined by Eq. (1):

$$\dot{m}_E = \frac{\dot{Q}_E}{\dot{q}_E} = \frac{\dot{Q}_E}{(h_1 - h_4)} \tag{1}$$

The compressor power consumption is determined from Eq. (2)

$$\dot{W}_{CR} = \dot{m}_E \cdot \dot{w}_{CR} = \dot{m}_E \cdot \left(\frac{h_{2s} - h_1}{\eta_{CS}} \right) \tag{2}$$

where η_{CS} is isentropic efficiency of the compressor. The isentropic efficiency is considered 0.85.

The condensation heat of the bottoming cycle $\dot{Q}_{CB}$ is determined as:

$$\dot{Q}_{CB} = \dot{m}_E \cdot \dot{q}_{CB} = \dot{m}_E \cdot (h_2 - h_3) \tag{3}$$

The condensation heat of the bottoming cycle $\dot{Q}_{CB}$ is rejected to the topping cycle refrigerant through the cascade condenser. This heat is the cooling load $\dot{Q}_{ET} = \dot{m}_S \cdot \dot{q}_{ET}$ for the topping cycle, thus $\dot{Q}_{CB} = \dot{Q}_{ET}$. Based on the heat balance of the cascade condenser, the following relationships can be made:

$$\dot{m}_E \cdot (h_2 - h_3) = \dot{m}_S \cdot (h_{12} - h_{11}) \tag{4}$$

From the relationship (4) the secondary mass flow rate of the topping cycle refrigerant $\dot{m}_S$ can be determined as:

$$\dot{m}_S = \frac{\dot{m}_E \cdot (h_2 - h_3)}{(h_{12} - h_{11})} = \frac{\dot{Q}_{CB}}{(h_{12} - h_{11})} = \frac{\dot{Q}_{ET}}{(h_{12} - h_{11})} \tag{5}$$

The ejector performance is evaluated by its entrainment ratio which is defined as the ratio of the mass flow rate of secondary to that of primary flow:

$$\mu = \frac{\dot{m}_S}{\dot{m}_P} \tag{6}$$

According to the conservation of energy, mass and momentum, and neglecting the inlet velocities of the

primary and the secondary flow, as well as velocity of the mixed flow at the exit of the diffuser, the ejector entrainment ratio μ can be expressed as [14]:

$$\mu = \sqrt{\eta_N \cdot \eta_M \cdot \eta_D \cdot \frac{(h_5 - h_6)}{(h_8 - h_7)}} - 1 \quad (7)$$

where η_N is isentropic efficiency of the nozzle, η_N= 0.85; η_M is isentropic efficiency of the mixing chamber, η_M=0.95; η_D is isentropic efficiency of diffuser, η_D=0.85 [14–16].

The mass flow rate of the primary flow $\dot{m}_P$ can be determined as:

$$\dot{m}_P = \frac{\dot{m}_S}{\mu} \quad (8)$$

The heat loads of the vapor generator $\dot{Q}_G$ and the condenser $\dot{Q}_C$ can be obtained from Eqs. (9) and (10), respectively:

$$\dot{Q}_G = \dot{m}_P \cdot \dot{q}_G = \dot{m}_P \cdot (h_5 - h_{10}) \quad (9)$$

$$\dot{Q}_C = (\dot{m}_P + \dot{m}_S) \cdot \dot{q}_C = (\dot{m}_P + \dot{m}_S) \cdot (h_8 - h_9) \quad (10)$$

The power consumption of the feed pump is given by:

$$\dot{W}_{FP} = \frac{\dot{m}_P \cdot v_9 \cdot (P_G - P_C) \cdot 10^3}{\eta_{FP}} \quad (11)$$

where η_{FP} is the efficiency of the feed pump.

The cascade system needs two types of power for operation: electrical power to drive the compressor $\dot{W}_{CR}$ and the feed pump $\dot{W}_{FP}$, and thermal power to drive the ejector $\dot{Q}_G$. Thus, the overall efficiency of the system can be characterized by two COPs: mechanical COP_{MECH} and thermal COP_{THRM}, which can be determined as:

$$COP_{MECH} = \frac{\dot{Q}_E}{\dot{W}_{CR} + \dot{W}_{FP}} \quad (12)$$

$$COP_{THERM} = \frac{\dot{Q}_E}{\dot{Q}_G} \quad (13)$$

2.3 The calculation of system design parameters and performance

The using of the cascade condenser for connecting the bottoming and the topping cycle allows choosing suitable refrigerant for the ejector cooling cycle to achieve maximum efficiency of the cascade system. R245fa was chosen as the refrigerant for the topping ERC in the present study. R245fa is a low-pressure refrigerant with positive-slope saturated-vapor line and has a high critical temperature. Its normal boiling point and the latent heat are 14.9°C and 196.23 kJ/kg, respectively; and it has a good application prospect, especially in air-conditioning at high evaporating temperatures [4, 17]. Meanwhile, refrigerant R245fa is also cheap, non-flammable and environmentally friendly with zero Ozone Depletion Potential (ODP).

To find the optimum design parameters, the cascade cooling cycle with cooling capacity $\dot{Q}_E$ =11.8 kW was theoretically investigated. The refrigerant R410a was used for the bottoming VCRC. The design evaporating temperature was T_E=5°C and the condensing temperature was T_C=45°C. The temperatures T_{CB} and T_{ET} are connected by the cascade condenser and are the objectives of the optimization as a core for the maximum efficiency of the cascade system. The results of the analysis are presented in Fig. 3 and Fig. 4.

First, the influence of the condensing temperature T_{CB} on the COP_{VCRC} of the VCRC was investigated. From Fig. 3, it indicates that with the condensing temperature decreasing from 45°C to 30°C, the COP_{VCRC} increases from 4.0 to 7.3, i.e. by 82.5%. Therefore, the reduction of condensing temperature is quite effective to improve the performance of VCRC.

Fig. 4 shows the variation in COP_{MECH} of the cascade system determined by Eq. (12) with evaporation temperature T_{ET} at different generator temperature T_G. The cooling capacity $\dot{Q}_E$ of the bottoming cycle is 11.8 kW. T_{CB} varies with the variation of T_{ET}. The temperature difference (T_{CB}–T_{ET}) between the condensation side and the evaporation side of the cascade condenser almost remains constant at 5°C. From Fig. 4, it presents that COP_{MECH} increases first, and then decreases with the increasing of the evaporating temperature T_{ET} of the ERC. The COP_{MECH} of cascade system reaches maximum values at T_{ET}=25°C. The compressor power consumption $\dot{W}_{CR}$ slightly increases due to the increasing of T_{CB}. At the same time, the mass flow rate of the primary flow $\dot{m}_P$ in the topping cycle decreases because the entrainment ratio increases with the increasing of T_{ET}. This leads the pump power consumption $\dot{W}_{FP}$ decreases rapidly. As a result, the COP_{MECH} increases for a given cooling capacity $\dot{Q}_E$ according to Eq. (12). When T_{ET} is higher than 25°C, the increasing in compressor power consumption $\dot{W}_{CR}$ is higher than the reduction of the pump power consumption $\dot{W}_{FP}$, and the COP_{MECH} decreases for a given cooling capacity $\dot{Q}_E$ according to Eq. (12).

The COP_{MECH} decreases with the increasing of generation temperature T_G of ERC for a given T_{ET} and $\dot{Q}_E$. Although the entrainment ratio increases and the flow rate of the primary fluid decreases, the pump power consumption $\dot{W}_{FP}$ increases owing to the increasing of pressure difference (P_G–P_C). Meanwhile, $\dot{W}_{CR}$ keeps constant. The low T_G can improve system performance in

general, and the high T_G allows work at high environmental temperature. Thus, T_{ET} and T_G should be optimized according to the operating conditions.

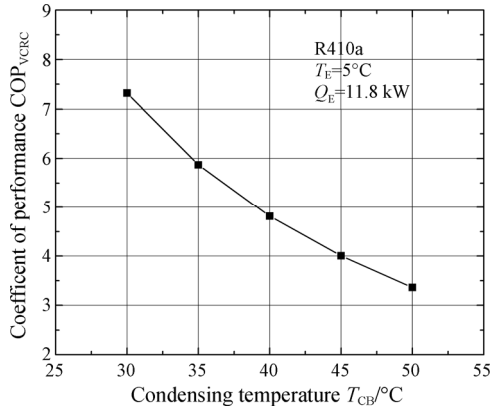

Fig. 3 The variation in COP_{VCRC} with condensing temperature

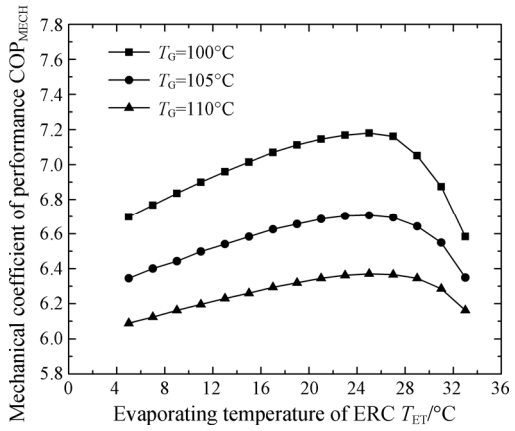

Fig. 4 The variation in COP_{MECH} of cascade refrigeration system with evaporating temperature of ERC

3. Description of an Experimental Setup and Procedure

To analyze the ejector and ejector refrigeration cycle at high evaporation temperatures, an ejector test rig with a cooling capacity of 15 kW was designed and built. Based on the theoretical analysis presented in Section 2, the design parameters for the ERC are as follows: the evaporating temperature T_{ET}=25°C, condensing temperature T_C=45°C, and the generating temperature T_G=110°C. The schematic diagram of the ERC test rig is shown in Fig. 5. The details of the main equipment are presented in Table 1.

The test rig equipment consists of the following major components: an ejector, a generator, an evaporator, a condenser, a needle expansion valve, a gear-type feed pump, a refrigerant receiver, a boiler, a steam condenser, a water chiller unit, regulating and stop valves, and a control panel equipped with different measurement instruments. A plate heat exchanger was used as the condenser to obtain the desirable test condition and lower the ejector backpressure. Shell and tube heat exchangers were employed as the generator and the evaporator. A gear-type pump was used in the test rig as the feed pump to achieve stable operation, especially when the pressure difference between generator and condenser was very high. The capacity of the feed pump could be adjusted by regulation of the pump motor speed through the inverter type regulator which can work at maximum 1.1 kW and an output frequency ranging from 0 to 60 Hz. The receiver served for collecting liquid refrigerant and ensuring its uninterrupted supply to the expansion valve and the feed pump. An electric boiler with rated heating power of 72 kW was used for generating steam to provide generator heat load. The steam condenser was used to liquefy steam exiting the generator. The generator heat load and generating temperature were controlled by regulating ball valves RBV5 and pump motor speed. Meanwhile, the ball valves RBV2 was used to regulate the flow rate of cold water through the steam condenser.

All heat needed to be rejected from the test rig was removed by cold water supplied from a water chiller unit. The cold water loop consisted of a water chiller unit, a cold water tank, a condenser, an evaporator and a heat exchanger. The condenser temperature and the ejector backpressure were controlled by varying the water flow through the condenser by regulating ball valves RBV1 and RBV3. The evaporator cooling load, evaporating temperature and pressure were adjusted by varying the expansion valve and the water flow through the evaporator by regulating ball valves RBV3 and RBV4.

Locations of measurement points around the circuit are shown in Fig. 5, and the measuring instruments are detailedly presented in Table 2. The temperature and the pressure sensors were placed at inlets and outlets of the evaporator, condenser, generator and ejector, transmitting output signals to a PC through a data acquisition unit.

The experimental ejector was designed by one-dimensional homogeneous equilibrium model and constant-pressure mixing model which was introduced by Keenan and Neumann [18] based on gas dynamics and was improved by Munday and Bugster [19] and later by Huang et al. [20]. The following assumptions are made for this model:

(1) The refrigerant flow is 1D steady-state flow and the heat transfer between flows and ejector walls are not taken into account;

(2) Velocities of streams at the ejector inlets and outlet are negligible;

(3) The frictional losses in the ejector nozzle, mixing chamber and diffuser are involved by using the coefficients of isentropic efficiency of these elements of the ejector.

The dimensions of the experimental ejector flow profile and its structure are presented in Fig. 6 and Table 3, respectively.

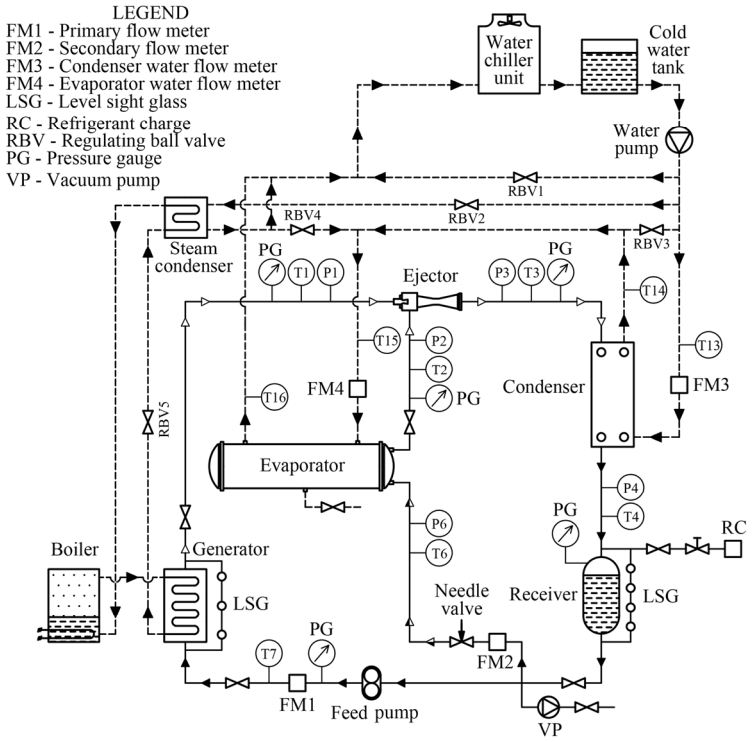

Fig. 5 Schematic diagram of the experimental test rig

Table 1 Details of the equipment

Items	Specifications
Condenser	50 kW plate heat exchanger (R245fa/water)
Generator	35 kW shell and tube heat exchanger (R245fa/steam)
Evaporator	20 kW shell and tube heat exchanger (R245fa/water)
Pump	Gear pump
Expansion valve	0.312″ (7.9 mm) HOKE's needle valve 3912F8B
Receiver	45L Stainless steel tank
Steam boiler	72 kW, 170°C steam with pressure 0.7 MPa max.
Water chiller unit	AUX water chiller, cooling capacity 65 kW

Table 2 Specifications of the measuring instruments

Required Measurements	Instruments	Range	Accuracy
Temperature	RTD sensor (Pt100)	−200°C to 350°C	±0.2°C
Pressure of primary fluid	Druck PT[a], UNIK 5000	(0 to 3.0) MPa	±0.2% FS[b]
Pressure of secondary fluid	Druck PT, UNIK 5000	(0 to 0.35) MPa	±0.2% FS
Outlet pressure of ejector	Druck PT, UNIK 5000	(0 to 1.6) MPa	±0.2% FS
Outlet pressure of condenser	Druck PT, UNIK 5000	(0 to 1.6) MPa	±0.2% FS
Inlet pressure of evaporator	Druck PT, UNIK 5000	(0 to 0.35) MPa	±0.2% FS
Inlet pressure of pump	Druck PT, UNIK 5000	(0 to 0.35) MPa	±0.2% FS
Primary mass flow rate	EMERSON Coriolis flow meter CMF050	(0 to 0.96) kg/s	±0.1% (Liquid, FS)
Secondary mass flow rate	EMERSON Coriolis flow meter CMF025	(0 to 0.302) kg/s	±0.1% (Liquid, FS)
Water mass flow rate through the condenser	EMERSON vortex flow meter 8600D	(0 to 9.6) kg/s	±0.8% (Liquid, FS)
Water mass flow rate through evaporator	EMERSON vortex flow meter 8600D	(0 to 6.0) kg/s	±0.8% (Liquid, FS)

[a]PT, Pressure transmitter; [b]FS, full scale.

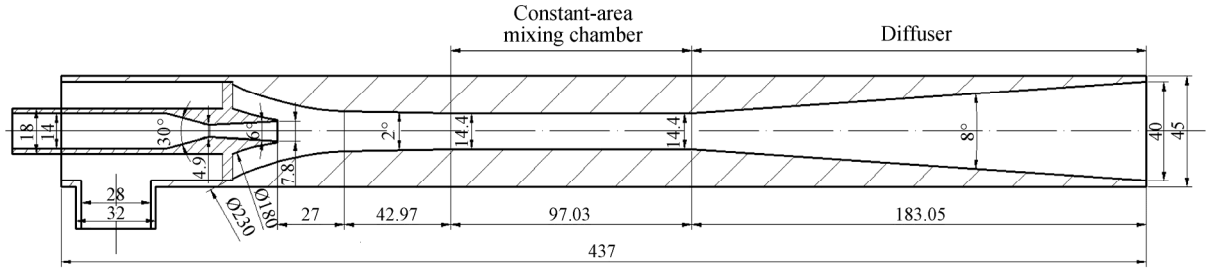

Fig. 6 Structure of the experimental ejector

Table 3 The geometric dimensions of the tested ejector

Throat diameter	4.9 mm
Nozzle exit diameter	8.8 mm
Diverging angle at nozzle exit	6.0°
Converging angle at nozzle enter	15.0°
Constant area section diameter	14.4 mm
Length of constant area mixing chamber	97 mm
Length of diffuser	183.05 mm
Diverging angle of diffuser	8°
Exit diameter of diffuser	40 mm

The experimental procedure is as follows:

(1) Check the cold water tank and make sure it is with plenty of water and satisfy circuit safety regulations;

(2) Turn on the measuring instruments and data collector for collecting the parameters including temperatures, pressures and flow rates;

(3) Confirm that each ball regulating valve is switched in a precise way and water can flow through the condenser, evaporator and steam condenser;

(4) Turn on the water chiller unit and boiler in sequence;

(5) Turn on the feed pump and control the primary mass flow rate of the refrigerant through the generator by inverter regulator to achieve needed generating temperature and pressure;

(6) When the system is running stable, control the evaporating temperature using the needle valve and regulating ball valves RBV3 and RBV4 to reach targeting cooling load;

(7) Adjust the water mass flow rate through the condenser by ball valves RBV1 and RBV3 to achieve the targeting condensation temperature;

(8) After 15 minutes of system stabilization, record the system parameters for one set, and after that, acquire the average of every ten sets for the final result;

(9) Change the operating conditions and repeat the procedure steps 5 to 8.

The expanded uncertainty of experimental results is calculated according to the detail information of sensors as [21]:

$$U = k \cdot u_Y = k \cdot \sqrt{\sum_i \left(\frac{\partial Y}{\partial x_i}\right)^2 \cdot u^2\left(x_i\right)} \tag{14}$$

$$Y = f\left(x_1, x_2, ...\right) \tag{15}$$

where k is the coverage factor; Y represents the performance parameters (COP, entrainment ratio and critical back pressure). The measured variable x_i includes temperatures, pressures and mass flow rates. All the estimated uncertainties were given in the experimental results section.

To compare the system performances under different operating conditions, the relative expanded uncertainty is defined and its calculation is shown in Eq. (16).

$$U_r = U \Big/ \left|Y\right| \tag{16}$$

4. Results and Discussion

The performance of the ejector and ERC was experimentally investigated under the following operating conditions: the evaporating temperature T_{ET} in the range of 15°C to 30°C, the condensing temperature T_C in the range of 40°C to 54°C, and the generation temperature T_G in the range of 100°C to 110°C.

According to the expanded uncertainty calculation shown in Eq. (16) and accuracy of the measuring instruments shown in Table 2, an error analysis is carried out to show the accuracy of measurement. The value of the coverage factor k here is chosen to be 3 with a 99% confidence interval [21]. The maximum relative expanded uncertainty of the COP_{THERM} of the ERC is about 0.6%. So, the detailed value of expanded uncertainty indicates that the accuracy of measurements in this study is acceptable.

Fig. 7 demonstrates the effect of the condensing temperature T_C on the ejector entrainment ratio μ, COP_{THERM} and cooling capacity $\dot{Q}_{ET}$ when generating temperature T_G varies from 100°C to 110°C given T_{ET}=30°C. From Fig. 7(a), it is seen that for each given T_G at lower T_C, the values of μ are not dependent on the ejector back pressure, i.e., the condensing temperature and pressure. This effect is closely related to the ejector's operating modes. This ejector mode is known as

"double-choking" or "critical" mode, which means the primary and secondary flows both choked and the entrainment ratio keeps constant until the back pressure reaches the critical point [20]. At the same time, if the condensing temperature T_C is higher than the value known as "critical condensing temperature", then μ, COP_{THERM} and $\dot{Q}_{ET}$ decrease quickly and then drop to zero. This ejector operating mode is called "single-choking" or "subcritical" mode. At this mode, the primary flow still choked, but the secondary flow is not choked [20].

From Fig. 7, it is presented that for the ejector with constant geometric profile, the critical values of the condensing temperatures T_C^* at unchangeable evaporating temperature T_{ET} are dependent on the generating temperature T_G. From the experimental results, it is suggested that at T_G=100°C, 105°C and 110°C, the values of T_C^* are equal to 44.8°C, 46.5°C and 47.7°C, respectively. At the same time, the critical values of COP_{THERM} decrease with T_G increasing. So, at T_G=100°C, 105°C and 110°C, the critical values of the entrainment ratio μ are 0.62, 0.56 and 0.47 (see Fig. 7(a)); the critical values of the COP_{THERM} are 0.45, 0.40 and 0.34 (see Fig. 7(b)), and the critical values of the cooling capacity $\dot{Q}_{ET}$ are 12.8 kW, 12.0 kW and 11.33 kW (see Fig. 7(c)), respectively. T_G could be adjusted by regulation of the pump motor speed through the inverter type regulator to meet the optimum operating conditions.

Fig. 8 shows experimental results for μ, COP_{THERM} and $\dot{Q}_{ET}$ measured at T_G=100°C and T_{ET}=15°C, 20°C, 25°C and 30°C, respectively. It can be seen that the trends of these measured parameters are almost the same as those presented in Fig. 7.

From Fig. 8, it is shown that for the ejector with constant geometric profile, the increase in evaporating temperature T_{ET} at unchangeable generation temperature T_G leads to a simultaneous increase of μ, COP_{THERM}, $\dot{Q}_{ET}$ and the critical condensing temperature T_C^*. Higher evaporation temperature helps to reduce the momentum difference between the primary and the secondary fluid in the mixing chamber of the ejector, thereby reducing irreversible losses and improving ejector operating efficiency. From Fig. 8(b), it is clear that the increase in evaporation temperature from 15°C to 30°C, the COP_{THERM} increases more than 137.1% from 0.190 to 0.451. The same significant increase is also observed for the cooling capacity $\dot{Q}_{ET}$ (see Fig. 8(c)). T_{ET} could be adjusted by regulation of the opening of the valve to meet the requirement of optimal operating conditions affected by ambient temperature. Along with the high critical condensing temperature T_C^*, this indicates the prospects of using the ejector refrigeration cycle as a topping cycle for the cascade refrigeration system.

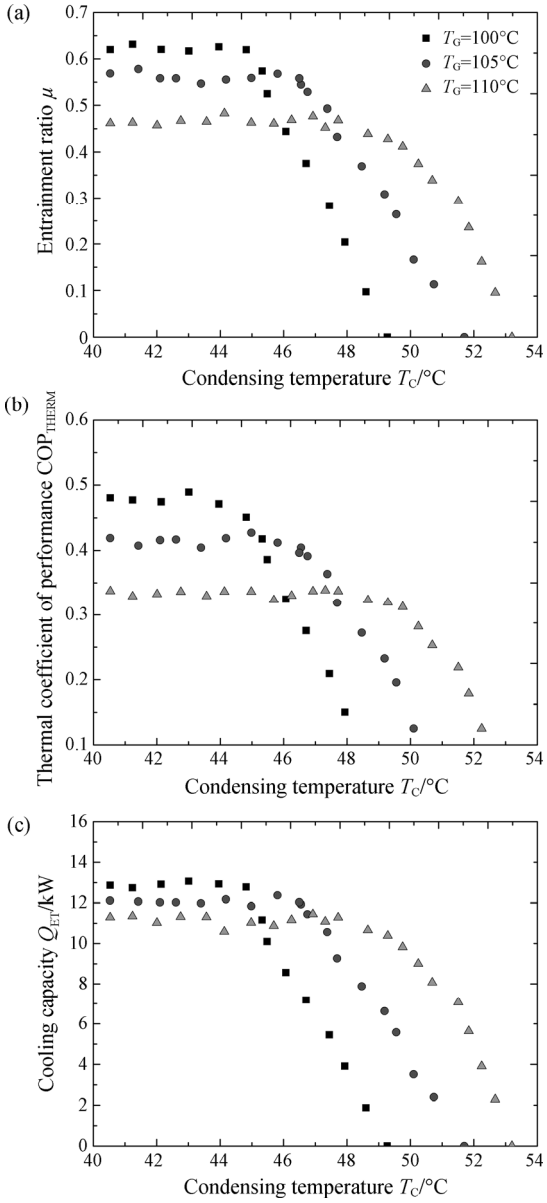

Fig. 7 Variations of (a) μ, (b) COP_{THERM} and (c) $\dot{Q}_{ET}$ with T_C at different T_G

Fig. 9(a) shows the relationship between measured critical condensing temperature T_C^*, evaporating temperature T_{ET} and generating temperature T_G based on experimental results. From Fig. 9(a), it can be seen that T_C^* increases with the increase in T_{ET} and T_G. So, at T_{ET}=30°C, the increase of T_G from 100°C to 110°C, the critical condensing temperature T_C^* increases from 44.8°C to 47.7°C accordingly. If T_{ET} changes from 15°C to 30°C at T_G=110°C, the critical condensation temperature T_C^* could increase from 43.9°C to 47.7°C.

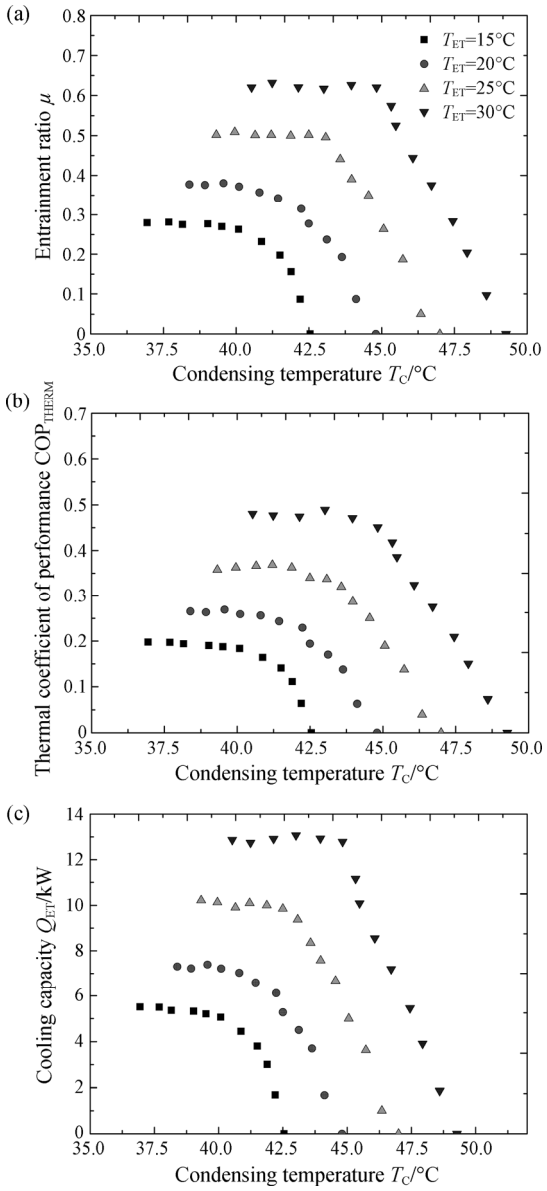

Fig. 8 Measured variations of (a) μ, (b) COP_{THERM} and (c) $\dot{Q}_{ET}$ with T_C at different T_E

Fig. 9(b) shows the measured data of COP_{THERM} at critical points under different T_G and T_{ET}. When the T_G=100°C and T_{ET}=20°C, the improvement of COP_{THERM} (taking the evaporating temperature of 15°C as the baseline) is 36.3%. While the improvement of COP_{THERM} (taking the evaporation temperature of 15°C as baseline) could be as large as 137.1% at T_{ET}=30°C. The higher T_G has a greater impact on the COP_{THERM} at the higher T_{ET}. To improve the performance of the system, T_{ET} can be properly increased and T_G can be lowered within a limited operating range. Experimental results and analysis in this study can be helpful for the application and operating condition optimization of ERC in cascade/hybrid refrigeration systems.

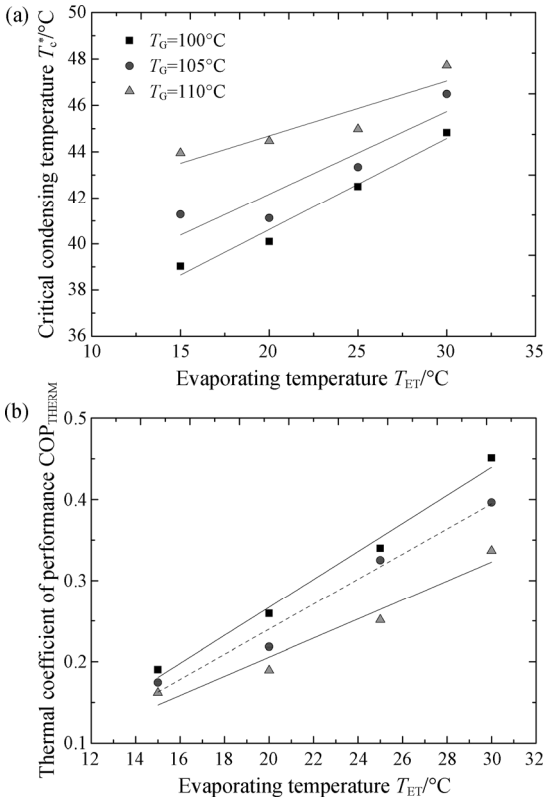

Fig. 9 Measured critical points in T_C^* (a) and COP_{THERM} (b) at different T_G and T_{ET}

5. Conclusions

In this paper, the ejector refrigeration cycle as a part of compression-ejector cascade refrigeration system was investigated. The theoretical analysis of the cascade cycle was carried out to find optimum operating conditions for the maximum improvement over the overall efficiency of the cycle. The experimental ejector refrigeration test rig was developed, built and investigated in a wide range of working conditions to determine their influence on the performance of the ejector cycle and find the ranges of its profitable operation.

The main conclusions of this study are summarized as follows:

(1) The theoretical analysis shows that ejector sub-cycle with high evaporation temperature is more beneficial to improve the overall performance of the cascade system. The maximum coefficient of performance of the cascade system occurs at the evaporation temperature of ERC 25°C;

(2) The high evaporation temperature improves the performance of ERC. The COP_{THERM} relative improvement of ERC (taking the evaporation temperature of 15°C as a baseline) is 137.1% at the evaporation temperature of 30°C. Performance improvement is very beneficial to the promotion and

application of ERC;

(3) For a constant ejector structure, the better COP_{THERM} and higher cooling capacity occur when the ejector works in critical mode at low generation temperature and high evaporation temperature;

(4) Lower generation temperature helps improve system performance at double-choked mode; however, the critical condensing temperature would also be lower which limits ejectors working at high ambient temperatures.

These results could be helpful to the application of ERC in cascade/hybrid system, including the optimum selection of operating conditions. Also, the high-quality experimental data for the ejector system at high evaporating temperatures which have not been reported before could be used to confirm the extrapolation reliability of different available theoretical models for ERC.

Acknowledgements

This work is financially supported by National Natural Science Foundation of China (NSFC) (Contract No. 51906216, No. 51706167) and Zhejiang Province Natural Science Foundation of China (Contract No. LY16E060004).

References

[1] Dupont J.L., The role of refrigeration in the global economy. 38th Informatory Note on Refrigeration Technologies, Informatory note, 2019, pp: 1–12. https://iifir.org/en/fridoc/142028.

[2] Xu Z.Y., Wang R.Z., Yang C., Perspectives for low-temperature waste heat recovery. Energy, 2019, 176: 1037–1043.

[3] Besagni G., Mereu R., Inzoli F., Ejector refrigeration: A comprehensive review. Renewable and Sustainable Energy Reviews, 2016, 53: 373–407.

[4] Wang X.H., Yan Y.Y., Wright E., Hao X.Y., Gao N., Prospect evaluation of low-GWP refrigerants R1233zd(E) and R1336mzz(Z) used in solar-driven ejector-vapor compression hybrid refrigeration system. Journal of Thermal Science, 2020, 30: 1572–1580. DOI: 10.1007/s11630-020-1297-z.

[5] Sokolov M., Hershgal D., Enhanced ejector refrigeration cycles powered by low grade heat, Part 1. System characterization. International Journal of Refrigeration, 1990, 13: 351–356.

[6] Sokolov M., Hershgal D., Solar-powered compression-enhanced ejector air conditioner. Solar Energy, 1993, 51: 183–194.

[7] Arbel A., Sokolov M., Revisiting solar-powered ejector air conditioner – the greener the better. Solar Energy, 2004, 77: 57–66.

[8] Sun D.W., Solar powered combined ejector-vapour compression cycle for air conditioning and refrigeration. Energy Conversion and Management, 1997, 38: 479–491.

[9] Ben Mansour R., Ouzzane M., Aidoun Z., Numerical evaluation of ejector-assisted mechanical compression systems for refrigeration applications. International Journal of Refrigeration, 2014, 43: 36–49.

[10] Petrenko V.O., Huang B.J., Shestopalov K.O., Ierin V.O., Volovyk, O.S., An advanced solar-assisted cascade ejector cooling/CO_2 sub-critical mechanical compression refrigeration system. The proceedings of the ISES Solar World Congress, Kassel, Germany, 28 August–2 September, 2011. DOI: 10.18086/swc.2011.20.20.

[11] Nesreddine H., Bendaoud A., Aidoun Z., Ouzzane M., Le Lostec B., Experimental investigation of an ejector-compression cascade system activated with low-grade waste heat. The proceedings of the 24th IIR International Congress of Refrigeration, Yokohama, Japan, August 16–22, 2015, Paper No.: 569.

[12] Sanaye S., Farvizi A., Refahi A., Rafiei Nejad M.V., A novel application of optimization and computational fluid dynamics methods for designing combined ejector-compressor refrigeration cycle. International Journal of Refrigeration, 2019, 108: 174–189.

[13] Chen G., Ierin V., Volovyk O., Shestopalov K., An improved cascade mechanical compression-ejector cooling cycle. Energy, 2019, 170: 459–470.

[14] Yu J., Ren Y., Chen H., Li Y., Applying mechanical subcooling to ejector refrigeration cycle for improving the coefficient of performance. Energy Conversion and Management, 2007, 48: 1193–1199.

[15] Hao X.Y., Wang L., Wang Z.W., Tan Y.Y., Yan X.N., Hybrid auto-cascade refrigeration system coupled with a heat-driven ejector cooling cycle. Energy, 2018, 161: 988–998.

[16] Huang B.J., Chang J.M., Empirical correlation for ejector design. International Journal of Refrigeration, 1999, 22: 379–388.

[17] Chen J., Havtun H., Palm B., Screening of working fluids for the ejector refrigeration system. International Journal of Refrigeration, 2014, 47: 1–14.

[18] Keenan J.H., Neumann E.P., A simple air ejector. Journal of Applied Mechanics, 1942(June), pp: A-75–A-81.

[19] Munday J.T., Bagster D.F., A new ejector theory applied to steam jet refrigeration. Industrial & Engineering Chemistry Process Design & Development, 1977, 16: 442–449.

[20] Huang B.J., Chang J.M., Wang C.P., Petrenko V.O., A 1-D analysis of ejector performance. International Journal of Refrigeration, 1999, 22: 354–364.

[21] Possolo A., The NIST simple guide for evaluating and expressing measurement uncertainty. Journal of Physics Conference Series, 2016. DOI: 10.1088/1742-6596/772/1/012024.